Reconstruction of an excited-state molecular wave packet with attosecond transient absorption spectroscopy

Yan Cheng,[1,2,3] Michael Chini,[1,2,3] Xiaowei Wang,[1,2,3,4] Alberto González-Castrillo,[5] Alicia Palacios,[5] Luca Argenti,[2,3,5] Fernando Martín,[5,6,7] and Zenghu Chang[1,2,3,*]

[1]*Institute for the Frontier of Attosecond Science and Technology (iFAST), University of Central Florida, Orlando, Florida 32816, USA*

[2]*Department of Physics, University of Central Florida, Orlando, Florida 32816, USA*

[3]*CREOL - The College of Optics and Photonics, University of Central Florida, Orlando, Florida 32816, USA*

[4]*Department of Physics, National University of Defense Technology, Changsha, Hunan 41000, China*

[5]*Departamento de Química, Módulo 13, Universidad Autónoma de Madrid, Madrid 28049, Spain*

[6]*Condensed Matter Physics Center (IFIMAC), Universidad Autónoma de Madrid, Madrid 28049, Spain*

[7]*Instituto Madrileño de Estudios Avanzados en Nanociencia, Cantoblanco, Madrid 28049, Spain*

(Received 11 May 2016; published 5 August 2016)

Attosecond science promises to allow new forms of quantum control in which a broadband isolated attosecond pulse excites a molecular wave packet consisting of a coherent superposition of multiple excited electronic states. This electronic excitation triggers nuclear motion on the molecular manifold of potential energy surfaces and can result in permanent rearrangement of the constituent atoms. Here, we demonstrate attosecond transient absorption spectroscopy (ATAS) as a viable probe of the electronic and nuclear dynamics initiated in excited states of a neutral molecule by a broadband vacuum ultraviolet pulse. Owing to the high spectral and temporal resolution of ATAS, we are able to reconstruct the time evolution of a vibrational wave packet within the excited $B'\,^1\Sigma_u^+$ electronic state of H_2 via the laser-perturbed transient absorption spectrum.

DOI: 10.1103/PhysRevA.94.023403

I. INTRODUCTION

Purely electronic processes in atoms and small molecules typically proceed on attosecond to few-femtosecond time scales, as dictated by the energy-level spacing between the ground and low-excited states [1]. In the absence of external degrees of freedom, electronic wave packets excited in atoms by an isolated attosecond pulse [2–4] or by strong-field ionization [5,6] exhibit a high degree of coherence [7] and can be probed via the photoelectron or transient absorption spectrum. In molecules [8–10], electronic excitation is accompanied by redistribution of charge and the subsequent rearrangement—rotation, torsion, bond elongation—of the nuclei, on a time scale of femtoseconds to picoseconds, which can ultimately lead to the breaking of chemical bonds. Recent advances in the generation of attosecond light pulses [11] and time-resolved spectroscopic techniques [12] have opened the possibility of attosecond photochemistry [13,14], wherein the initial electronic excitation can steer a chemical reaction along a particular trajectory.

In the quantum dynamics of systems with chemical and biological interest, a major role is played by bound states. So far, pioneering experiments have demonstrated attosecond control of dissociation [9] and ionization [10] of hydrogen molecules by detecting the charged reaction products. As these techniques require passage through an ionization or dissociation step, however, the reconstruction of the dynamics occurring within the bound-state manifold from the final products is challenging. This is all the more true if photofragment detection techniques are used to investigate large systems, such as a chromophore within an extended molecule, as in this case one must also account for the interaction of the fragments with the atoms surrounding the reaction center. On the other hand, attosecond transient absorption spectroscopy (ATAS) is sensitive to the dynamics in individual bound states without the need for subsequent ionization or dissociation and therefore does not require disentangling the many pathways of electrons leading to fragmentation. With the availability of high-resolution VUV spectrometers [15], one can conceivably monitor the recurrence of the vibronic wave packet created close to a localized reaction center, even in solution. ATAS has already been applied successfully to selected studies of strong-field ionization [5] and dissociation [16], wave-packet motion [3,4,6,17,18], and correlated electron dynamics [19–22], as well as phase transition dynamics in condensed matter [23,24], with unprecedented energy and time resolution. As ATAS encodes both the amplitudes and phases of interacting states, reconstruction and control of an electron wave packet—in both space and time—has been achieved [22]. With these developments in both experimental and theoretical approaches, it is becoming ever more apparent that ATAS has general applicability to a wide range of dynamical processes.

In this work, we report the reconstruction of the time-dependent molecular wave packet in an excited state of H_2 from the measured ATAS signal. Through measurements employing synchronized subfemtosecond VUV pulses and few-cycle near-infrared (NIR) laser pulses, we monitor the absorption spectrum in the spectral region spanning the bound excited-state manifold of H_2 and detect clear evidence of electronic coherences and ultrafast recurrences associated with entangled electronic-nuclear wave packets. The experiments are accompanied by state-of-the-art *ab initio* quantum calculations, which fully account for both the electronic and nuclear motion in the presence of the two pulsed fields, and which guide the interpretation of the rich dynamics through the development of few-level models that include the minimum number of electronic states required to reproduce the most

*Zenghu.Chang@ucf.edu

relevant features observed in the experimental and the fully *ab initio* results. Based on these models, we develop a procedure to reconstruct, from the measured ATAS, the VUV-induced molecular wave packet on an excited electronic state, finding good agreement with theoretical predictions. These results demonstrate the capability of ATAS to resolve the wave-packet dynamics in a neutral molecule, for which attosecond electron excitation triggers nuclear motion evolving on the manifold of potential energy surfaces and provides a realistic pathway towards measurement of coherent electronic and nuclear wave-packet dynamics in larger molecules [25–27].

II. HOLOGRAPHIC PRINCIPLE

One way to describe the time evolution of a wave packet $\psi(R,t)$ is to express it in terms of the eigenstates of the field-free Hamiltonian, $H_0\phi_n(R) = E_n\phi_n(R)$, i.e., $\psi(R,t) = \sum_n c_n(t)\phi_n(R)$. In this representation, once the spectral amplitudes $c_n(t)$ are determined at a given time t_0, it is possible to compute their value at any subsequent time using the relation $c_n(t) = c_n(t_0)e^{-iE_n(t-t_0)/\hbar}$. While this approach has been successfully used to reconstruct the dynamics of a metastable wave packet in the helium atom [22], it has limitations. Namely, to reconstruct the wave packet in space, one must know beforehand both the energies E_n and the functions $\phi_n(R)$.

In principle, the wave packet $\psi(R,t)$ can be expressed in any complete orthogonal basis $\chi_n(R)$, $\psi(R,t) = \sum_n q_n(t)\chi_n(R)$, where $q_n(t) = \int^d R\chi_n^*(R)\psi(R,t)$. Compared to the previous case, the expansion coefficients $q_n(t)$ do not have a trivial time dependence anymore. To reconstruct the wave-packet dynamics, therefore, the $q_n(t)$ must be measured as a function of time. On the other hand, if the basis functions $\chi_n(R)$ are known at the outset, it is possible to reconstruct the wave packet even if the eigenstates $\phi_n(R)$ cannot be observed or computed. This second approach, therefore, is especially useful in the case of vibrational wave packets on excited potential energy surfaces, for which the eigenstates may be difficult to map experimentally or even to compute theoretically.

In this work, we follow the second approach to reconstruct the fast dynamics of a nuclear wave packet in the B' excited bound electronic state of the H_2 molecule. Rather than basing the reconstruction on the knowledge of the B' vibrational states, we determine its expansion in terms of the bound vibrational states of a lower B electronic level. The principle is illustrated in Fig. 1. From the $X\,^1\Sigma_g^+$ ground state, a VUV pulse excites coherently two vibrational wave packets, on the B and $B'\,^1\Sigma_u^+$ manifolds, which begin to evolve independently. After a delay τ, a short IR probe pulse promotes, by means of a two-photon transition, a small portion of the vibrational wave packet from one electronic potential energy surface to the other. Therefore, the time-dependent amplitude $c_{\nu_B}(t;\tau)$ of the $|B\ \Sigma_u^+\rangle \otimes |\nu_B\rangle$ vibronic state, which within the adiabatic approximation is given by the product of an electronic and a vibrational wave function, receives two contributions, $c_{\nu_B}(t;\tau) = c_{\nu_B}^{(1)}(t) + c_{\nu_B}^{(3)}(t;\tau)$. One, $c_{\nu_B}^{(1)}(t)$, is the first-order amplitude due to the absorption of a VUV photon from the ground state, whereas $c_{\nu_B}^{(3)}(t;\tau)$ is due to the third-order sequential process comprising the initial

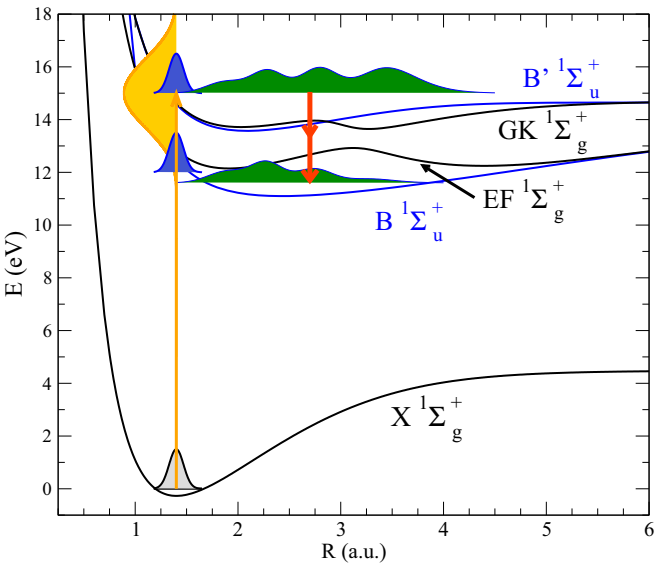

FIG. 1. Potential energy curves for the ground electronic state and the first two singly excited $^1\Sigma_u^+$ (blue curves) and $^1\Sigma_g^+$ (green curves) states of the hydrogen molecule. The molecule, initially in its ground electronic and vibrational state (gray shaded area), is excited by a subfemtosecond VUV pulse (orange arrow), which has a broad spectrum (orange shaded area), to a coherent superposition of excited vibrational wave packets in both the B and B' electronic states. (Here, we assume the molecule is aligned to the laser polarization.) According to the Franck-Condon principle, the two excited vibrational wave packets (blue shaded areas) are initially aligned with the ground-state wave packet. However, since they are subject to different potential energy surfaces, they rapidly undergo separate evolution (green shaded areas). After a time delay $\boldsymbol{\tau}$, the NIR pulse promotes an exchange of population between the two excited $^1\Sigma_u^+$ manifolds (red arrows), assisted by the EF and GK $^1\Sigma_g^+$ states.

excitation of a vibrational wave packet on the B' manifold $|B'\ \Sigma_u^+\rangle \otimes |\chi_{B'}(t)\rangle$, with $|\chi_{B'}(t)\rangle = \sum_\nu c_{\nu_{B'}}^{(1)}(t)|\nu_{B'}\rangle$, followed by the stimulated emission of two NIR photons.

The time scale $\sigma_{\rm NIR}$ of the second transition is determined by the duration of the NIR probe pulse. For extremely short probe pulses, this transition can occur on a time scale much shorter than that of the evolution of the vibrational wave packets on either surfaces, such that the wave packet promoted to the B surface is a replica of that on the B' surface at time τ multiplied by a two-photon dipole transition amplitude with a smooth radial dependence. Indeed, the term $c_{\nu_B}^{(3)}(t;\tau)$ is given by the coherent contribution of all the components of the upper wave packet, evaluated at the arrival time of the NIR pulse:

$$c_{\nu_B}^{(3)}(t;\tau) \cong e^{-i\omega_{\nu_B,g}(t-\tau)}\Phi\left(\frac{t-\tau}{\sigma_{\rm NIR}}\right)\sum_{\nu_{B'}}\mathcal{A}_{\nu_B\leftarrow\nu_{B'}}^{(2)}c_{\nu_{B'}}^{(1)}(\tau), \quad (1)$$

where $\omega_{\nu_B,g}$ is the energy difference between the ground and the B vibronic state, and the smooth step function $\Phi(x)$ is defined as $\Phi(x) = (2\pi)^{-1/2}\int_{-\infty}^{x} e^{-t^2/2}dt$. $\mathcal{A}_{\nu_B\leftarrow\nu_{B'}}^{(2)}$ is a second-order transition probability amplitude for the two-photon transition mediated by the EF and GK $^1\Sigma_g^+$ states. The analytical expression for $\mathcal{A}_{\nu_B\leftarrow\nu_{B'}}^{(2)}$ is immaterial to the present discussion. Here, we simply note that the short duration of the NIR pulse allows us to factorize this amplitude into an

electronic component $\mathcal{A}^{(2)}_{B\leftarrow B'}$ and a Franck-Condon overlap,

$$\mathcal{A}^{(2)}_{v_B\leftarrow v_{B'}} \cong \mathcal{A}^{(2)}_{B\leftarrow B'}\,\langle v_B|v_{B'}\rangle, \tag{2}$$

where we neglect the dependence of the electronic dipole moment on the internuclear distance R. The coefficients $c^{(3)}_{v_B}(t;\tau)$ then become

$$c^{(3)}_{v_B}(t;\tau) \cong e^{-i\omega_{v_B,g}(t-\tau)}\Phi\left(\frac{t-\tau}{\sigma_{\rm NIR}}\right)\mathcal{A}^{(2)}_{B\leftarrow B'}\langle v_B|\chi_{B'}(\tau)\rangle. \tag{3}$$

Equation (3) indicates that the B' time-dependent wave packet is holographically imprinted on the B vibrational states, with weights proportional to the vertical-transition factors $\langle v_B|\chi_{B'}(\tau)\rangle$. In other words, we can identify the time-dependent amplitudes and phases of the beating of the B vibrational peaks in the transient absorption spectrum with the instantaneous amplitudes of the vibrational components of the wave packet in the B' state, and thus reconstruct the whole nuclear dynamics in the excited manifold.

III. METHODS

A. Experimental setup

In the experiments, few-cycle (∼5-fs) pulses with a central wavelength of 730 nm from a Ti:sapphire amplifier with a hollow-core fiber and chirped mirror pulse compressor were focused using a spherical mirror ($f = 500$ mm) into a quasistatic gas cell (inner diameter 1.2 mm) with laser-drilled holes placed ∼5 mm after the laser focus. Broadband VUV pulses with spectrum supporting a transform-limited pulse duration of 750 asec, which were generated using the generalized double optical gating technique [28] in low-pressure xenon gas (typically 1–5 mbar) and synchronized few-cycle NIR laser pulses with a variable time delay were combined with a hole-drilled mirror and focused together into a second quasistatic gas cell (inner diameter 1.5 mm) filled with ∼20 mbar of H_2 gas. The peak intensity of the NIR laser was $\sim 5\times 10^{12}$ W/cm^2. The spectral range of the VUV pulses was selected using an indium foil filter placed after the first gas cell with transmission extending ∼12–17 eV, which overlaps with the excited-state manifold of neutral H_2. After passing through the gas cell, the VUV spectrum was dispersed using a flat-field grazing-incidence spectrometer with a spectral resolution of ∼40 meV at 15 eV. The delay was scanned using a mirror mounted on a piezoelectric stage and was actively stabilized to an error of ∼25 asec RMS during the experiments. Details of the experimental setup can be found in previous publications [4,29] and references therein.

B. Quantum calculations

The attosecond transient absorption cross section $\sigma_{TAS}(\omega;\tau,\mathbf{\Omega})$ of a molecule with the internuclear axis oriented along $\mathbf{\Omega}$, expressed as a parametric function for the pump-probe time delay τ, is

$$\sigma_{TAS}(\omega;\tau,\mathbf{\Omega}) = \frac{4\pi}{c\omega}\mathrm{Im}\left[\frac{\tilde{p}(\omega;\,\tau,\mathbf{\Omega})}{\tilde{A}_{VUV}(\omega;\,\tau)}\right], \tag{4}$$

where $A_{VUV}(t;\tau)$ is the amplitude of the VUV component of the external vector potential, which is assumed to be polarized along the $\hat{z}$ direction, $p(t;\,\tau,\mathbf{\Omega}) = \langle\psi(t)|\hat{z}\cdot\vec{p}|\psi(t)\rangle$ is the expectation value of the total electronic canonical momentum along the VUV polarization, and, for both quantities, $\tilde{f}(\omega) = (2\pi)^{-1/2}\int dt\;\; f(t)e^{i\omega t}$ indicates the corresponding Fourier transform (FT) [30]. In Eq. (1), the NIR dressing pulse defines the time origin, while the VUV pulse depends parametrically on the time delay τ as $A_{VUV}(t;\tau) = A_{VUV}(t-\tau;0)$, so that $\tilde{A}_{VUV}(\omega;\,\tau) = e^{i\omega\tau}\tilde{A}_{VUV}(\omega;\,0)$. Thus, the molecular dipole moment and, in turn, the cross section, depend on the time delay, on the molecular orientation, and on the full spectra of the NIR and VUV pulses.

The time-dependent wave function $|\psi(t)\rangle$ resulting from the interaction of the external pulses with the molecule in its ground electronic and vibrational state $|g\rangle$ is computed *ab initio* by expanding it in a large basis of Born-Oppenheimer (BO) molecular states (see Refs. [8] and [31] for more details). The method includes all electronic and vibrational (dissociative) degrees of freedom and therefore accounts for electron correlation and the nuclear motion. The BO basis includes the six lowest bound states and a set of discretized continuum states for each of the following symmetries: $^1\Sigma_g{}^+$, $^1\Sigma_u{}^+$, $^1\Pi_g$, $^1\Pi_u$, and $^1\Delta_g$. All bound-bound and bound-continuum dipole couplings have been included. In the simulation we have used a VUV pulse of central frequency 15 eV, duration at half maximum 400 asec, and intensity 10^{10} W/cm^2, and an IR pulse of, respectively, 1.7 eV, 4 fs, and 2×10^{12} W/cm^2. Both pulses have a sine-squared envelope and carrier-envelope phase of 0°. Due to the finite size of the boxes used in the evaluation of the wave function, time integration could only be performed up to 22 fs, which limits our calculations to time delays from −20 to +20 fs.

To compute $\tilde{p}(\omega)$ (we omit specification of parametric dependences, unless necessary), we need $p(t)$ at arbitrarily long time. In the presence of external fields, the observable $p(t)$ is evaluated numerically. As soon as the external fields are over, $p(t)$ is exactly known since the wave function is expressed in a basis of eigenstates of the field-free Hamiltonian. In the spectral range between 10 eV and 20 eV, the dipolar response of the system entails only beatings between the ground state and excited components with either Σ_u or Π_u symmetry, in the parallel and perpendicular orientation, respectively. Owing to the weak intensity of the subfemtosecond VUV pulse, the ground-state population is hardly affected and can thus be assumed to be 1. We take into account the random orientation of the molecules by approximating the transient absorption cross section as a weighted average of the cross sections in the parallel and orthogonal orientations, $\sigma_{TAS,\parallel}(\omega;\tau) = \sigma_{TAS}(\omega;\tau,\hat{z})$ and $\sigma_{TAS,\,\perp}(\omega;\tau) = \sigma_{TAS}(\omega;\tau,\hat{x})$, respectively:

$$\sigma_{TAS}(\omega;\tau) \cong \tfrac{1}{3}\sigma_{TAS,\parallel}(\omega;\tau) + \tfrac{2}{3}\sigma_{TAS,\perp}(\omega;\tau). \tag{5}$$

IV. RESULTS

The bound-state manifold of molecular hydrogen [32] is plotted in Fig. 2(a). Following the interaction of a gaseous sample of hydrogen molecules with a subfemtosecond VUV pulse, dense bands of absorption lines corresponding to the electronic and vibrational excitation of neutral hydrogen molecules are imprinted on the continuum spectrum, as shown in Fig. 2(b).

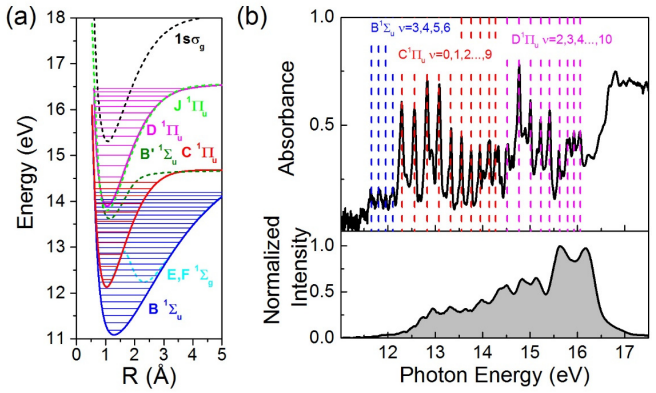

FIG. 2. (a) The hydrogen bound-state manifold consists of several vibronic state manifolds. Electronic excited states relevant to the present study are labeled. (b) Absorption lines corresponding to the $B\,^1\Sigma_u^+ \leftarrow X\,^1\Sigma_g^+$, $C\,^1\Pi_u \leftarrow X$, and $D\,^1\Pi_u \leftarrow X$ bands of neutral hydrogen molecules can be observed in the attosecond spectrum. The spectrum was obtained with the NIR pulse arriving on the target prior to the VUV pulse ($\tau \approx +30$ fs). The spectral range of the VUV pulse (lower panel) was selected by using an indium foil filter.

The most prominent features in the ATAS spectrum originate primarily from the excitations $B\,^1\Sigma_u^+ \leftarrow X\,^1\Sigma_g^+$, $C\,^1\Pi_u \leftarrow X$, and $D\,^1\Pi_u \leftarrow X$, as indicated in Fig. 2(b), in good agreement with photoabsorption measurements made using incoherent VUV continuum sources [33]. In the presence of the perturbing NIR laser field, the absorption line strengths, energies, and shapes are observed to change with the time delay between the XUV and NIR pulses. Figures 3(a) and 3(b), respectively, depict the experimentally measured and *ab initio* calculated delay-dependent absorbance of the H_2 target in the vicinity of the bound-state manifold, where negative (positive) time delays indicate that the VUV pulse arrives on the target before (after) the peak of the NIR laser envelope.

Both the experimental and calculated ATAS exhibit features which evolve on two different time scales. First, we note the presence of fast modulations in the delay-dependent absorption with a periodicity of ∼1 fs. These modulations are present at all photon energies in the vicinity of zero delay (VUV-NIR overlap) but also persist to large negative delays, particularly in the vicinity of the $B \leftarrow X$ transitions and above the ionization threshold. Second, we observe features which vary more slowly, most obviously in the vicinity of the $C\,^1\Pi_u$ states. These features, and the molecular dynamics which they encode, will be discussed in detail in Sec. V. There are differences between the measured and calculated ATAS spectra, both in the global shape of the absorption spectrum (i.e., relative strengths of the $B \leftarrow X$, $C \leftarrow X$, and $D \leftarrow X$ transitions) and in the observed delay dependences. In particular, the highest optical density band in the experiments appears approximately 1 eV above that in the time-dependent Schrödinger equation (TDSE) calculation. These differences can be attributed to the use of a dense gas target in the experiments, needed to resolve the weak absorption features corresponding to the $B \leftarrow X$ transitions. Indeed, it is known that direct photoabsorption measurements do not yield accurate absorption cross sections for discrete transitions [34], primarily due to line saturation effects, and the calculated field-free absorption cross section is in excellent agreement with accurate measurements using electron-energy-loss spectroscopy [35]. Furthermore, recent studies have shown that temporal reshaping of the VUV pulse, which accompanies photoabsorption in dense gas targets, may distort the delay-dependent features in ATAS [36–38]. Both of these issues can in principle be overcome through the use of a higher-resolution VUV spectrometer, which would permit the use of lower gas pressures. As we will show below, the measured ATAS spectrum already allows us to reconstruct the time-dependent molecular wave packet resulting from the VUV excitation.

V. DISCUSSION

When the VUV pulse arrives on the target first, the ATAS spectrum exhibits delay-dependent changes in the absorption line energies, shapes, and strengths. In general, these features can be attributed to a process wherein the broadband VUV pulse induces a time-dependent dipole response in the molecular target, which is perturbed by the NIR field. The mechanism of the laser perturbation can be further classified by scrutinizing the absorption dynamics within a particular excited-state absorption line: resonant processes involving coupling of neighboring states through the absorption or emission of one NIR photon typically result in relatively slowly varying spectral features such as absorption line splitting (analogous to Autler-Townes splitting [39]) and perturbed free induction decay [40], whereas nonresonant couplings involving two or more NIR photons result in fast oscillations with periodicity shorter than the dressing laser optical cycle [4]. These features reveal information about the field-free evolution of the electronic wave packet in the interval between the two pulses [2,41,42]. In the case of molecules, dipole absorption reflects nuclear dynamics as well [18]. According to the adiabatic approximation [43], the electronic response to the nuclear motion is instantaneous. In an electronic transition promoted by the NIR probe pulse, therefore, all the vibrational levels that belong to the same electronic state populated by the VUV contribute in proportion to their instantaneous amplitude, such that the time-dependent dipole is further modulated on the time scale of the nuclear vibrations. This modulation can be observed in ATAS as relatively slow oscillations on the time scale of the nuclear vibration.

By comparing Figs. 3(a) and 3(b), we identify two regions in which the nuclear motion within a particular electronic state can be discerned from slow modulations in the experimental ATAS spectra, corresponding approximately to the $C \leftarrow X$ (13.0–14.0 eV) and $B \leftarrow X$ (11.0–12.5 eV) bands. Figures 3(c) and 3(e) show individually the ATAS spectra in these two regions over a longer range of delays. In each of these regions, recurrent absorption line structures (splitting, shifting, and modulation) are observed with periodicity approximately equal to the full vibrational period of the associated state, in qualitative agreement with the calculated ATAS spectra. These recurrent structures correspond to coherences between consecutive vibrational components of the nuclear wave function and indicate the state-resolved observation of the nuclear wave packet evolving on each distinct potential energy surface. The ability to differentiate these signatures of the

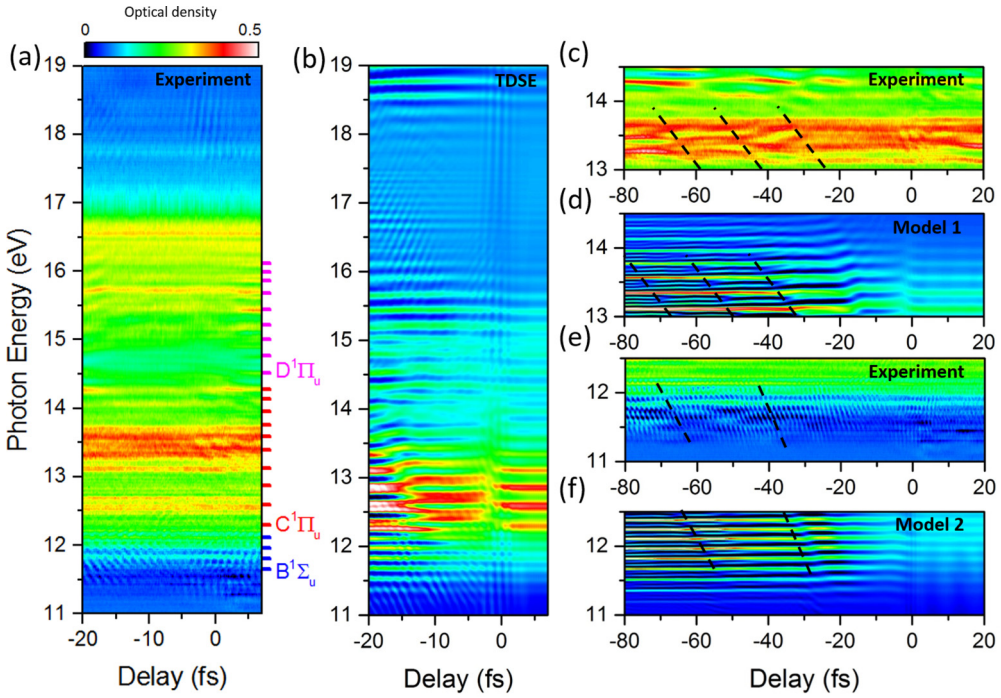

FIG. 3. (a) Experimental measurement and (b) *ab initio* quantum simulations of the delay-dependent absorption spectrum of hydrogen molecules near delay zero. The vibrational levels of the $B\,^1\Sigma_u^+$ ($v = 3-6$), $C\,^1\Pi_u$ ($v = 0-9$), and $D\,^1\Pi_u$ ($v = 2-10$) states are shown in panel (a). (c, d) The measured and simulated ATAS spectrum in the vicinity of the $C\,^1\Pi_u$ states, while (e) and (f) show the measured and simulated ATAS spectrum in the vicinity of the $B\,^1\Sigma_u^+$ states. The model calculations shown include only the $X\,^1\Sigma_g^+$ ground state and (c), the $C\,^1\Pi_u$ and $J\,^1\Delta_g$ and (e), excited $B\,^1\Sigma_u^+$, $EF\,^1\Sigma_g^+$, and $B'\,^1\Sigma_u^+$ bound states excited states. The dashed lines in panels (c)–(f) serve to guide the eye to periodic structures associated with the vibrational wave packets in the $C\,^1\Pi_u$ (∼20 fs periodicity) and $B\,^1\Sigma_u^+$ (∼25–30 fs periodicity) states.

electronic and nuclear dynamics in individual excited states suggests the applicability of ATAS to resolve multiscale dynamics in larger molecular systems.

The *ab initio* quantum calculations can provide valuable insight into the ATAS measurements by identifying the primary coupling pathways for each electronic state. This allows for the development of model systems including only a few molecular states, for which the transient absorption spectrum can be calculated for arbitrarily long time delays while fully accounting for the nuclear motion. Two such model calculations, in which the basis has been restricted to the ground $X\,^1\Sigma_g^+$ state and either (i) the excited $C\,^1\Pi_u$ and $J\,^1\Delta_g$ bound states or (ii) the excited $B\,^1\Sigma_u^+$, $EF\,^1\Sigma_g^+$ and $B'\,^1\Sigma_u^+$ bound states, are shown in Figs. 3(d) and 3(f), respectively. These are the only states required to account for the bound motion triggered by the VUV in the excited state. Dealing with only bound states, furthermore, simplifies the theoretical analysis, since the calculations can easily be extended to very long times. The first model is appropriate for molecules oriented perpendicular to the polarization direction and can be compared to the transient absorption in the vicinity of the $C \leftarrow X$ transition [Figs. 3(c) and 3(d)], while the second model is appropriate for molecules oriented parallel to the polarization direction and can be compared to the transient absorption in the vicinity of the $B \leftarrow X$ transition [Figs. 3(e) and 3(f)]. As can be seen, the absorption line dynamics follow the vibrational periods of the excited states; furthermore, the absorption lines in the vicinity of the $B \leftarrow X$ transition exhibit ∼1 fs beating associated to two-photon IR-induced transitions between the B' and B states mediated by the EF state [Figs. 3(e) and 3(f)].

The vibrational peaks in the ATAS spectrum exhibit periodic modulations as a function of the pump-probe delay at multiples of the vibrational periods, as observed also in Ref. [44]. These modulations result from the interference between the hyperbolic fringes associated to different nearby vibrational states. These fringes reflect the local alteration of the vibrational state amplitude caused by the interaction with the IR probe field, which depletes or otherwise modifies the field-free evolution of the state.

To support this interpretation, we have used a minimal model that includes the ground $|X\ \Sigma_g^+\rangle \otimes |0_X\rangle$ state, and the $|C\ \Pi_u\rangle \otimes |v_C\rangle$ and $|J\ \Delta_g\rangle \otimes |v_J\rangle$ excited states to evaluate the transition amplitude to the C state. This model is similar to that described in Sec. II, except for the fact that we are now considering the C state being depleted by the one-photon transition to the J state, instead of the B state being populated by a two-photon transition from the B' state. The vibrational states $|v_C\rangle$ of the $C\,^1\Pi_u$ electronic state are excited in a short time interval σ_{VUV}, comparable to the duration of the VUV pump pulse. The NIR-induced transition to the J state simply depletes the C-state amplitude after a delay τ by the NIR probe pulse. Under these circumstances, the amplitude associated with the latter transition can be assumed to be a constant ϵ with $0 \leqslant \epsilon \leqslant 1$. Hence the resulting transition amplitude to the C state including these one- and two-photon paths can be

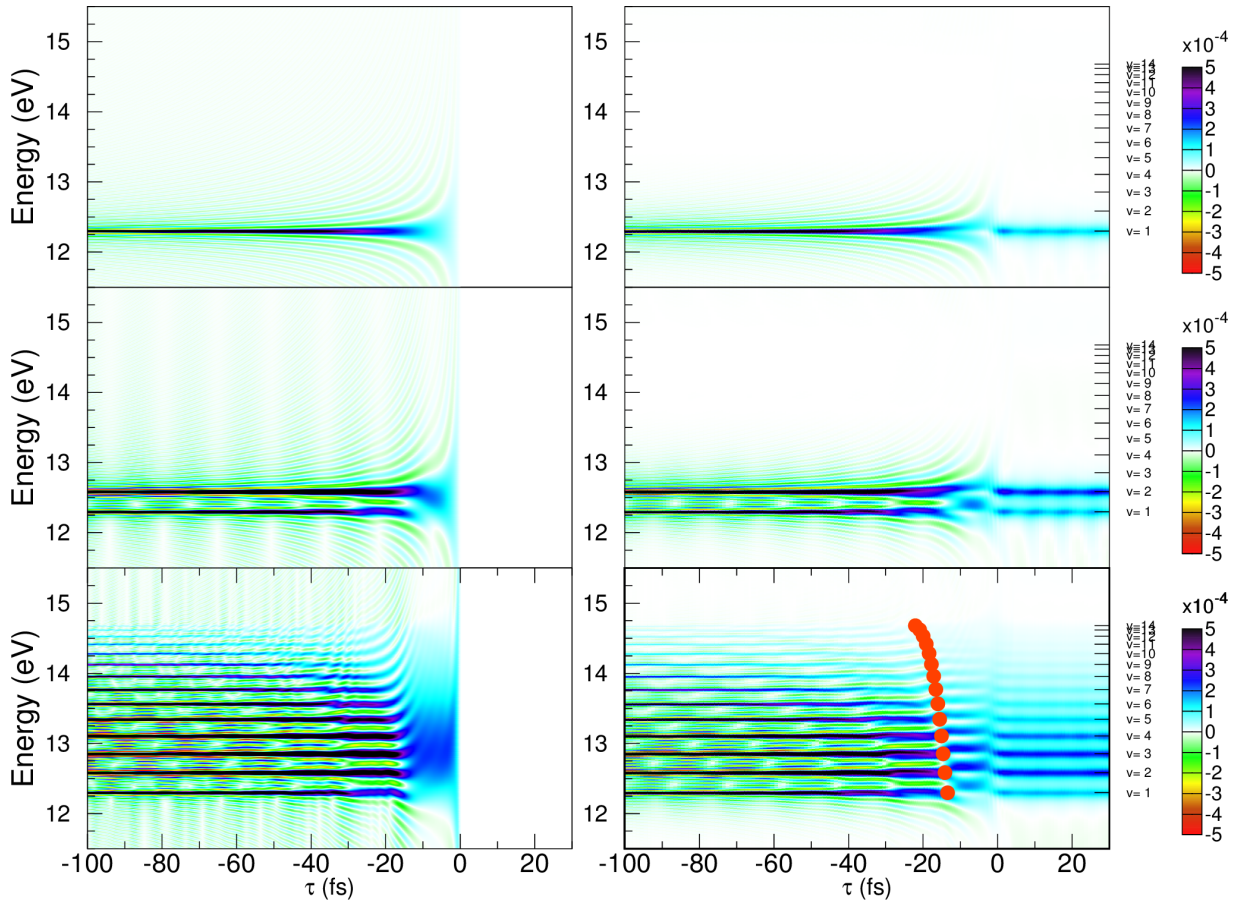

FIG. 4. ATAS spectra computed with the simple model described in the text (left panels) as well as *ab initio* with a restricted $C\ ^1\Pi_u$ spectral basis (right panel). In each case, the $C\ ^1\Pi_u$ manifold is comprised (top to bottom) of one, two, and all the vibrational levels. The red circles in the bottom-right panel indicate the corresponding vibrational periods.

written

$$c_{v_C}(t) = F\left(\omega_{v_C,g}\right)\left[1 - \epsilon\Phi\left(\frac{t-\tau}{\sigma_{\rm NIR}}\right)\right] \times \Phi\left(\frac{t}{\sigma_{VUV}}\right)\langle v_C|0_X\rangle e^{-i\omega_{v_C\ g}t}, \quad (6)$$

where we have assumed the Franck-Condon approximation. The factor $F(\omega_{v_C\ g})$ accounts for the VUV pulse spectrum and the dipole transition matrix element between the ground and Π_u state,

$$F\left(\omega_{v_C,g}\right) = \frac{2\pi}{i}\tilde{A}_{VUV}\left(\omega_{v_C\ g}\right)\langle C\ \Pi_u|p_z|X\ \Sigma_g^+\rangle(R_{eq}), \quad (7)$$

where R_{eq} is the equilibrium nuclear distance in the ground electronic state. Here we are interested in the depletion effects induced by the NIR, however small, so we can take just $\epsilon = 1$ for simplicity. The time-dependent expectation value of the canonical momentum is then proportional to

$$p(t;\ \tau) \propto \Phi\left(\frac{t-\tau}{\sigma_{\rm NIR}}\right)\Phi\left(\frac{t}{\sigma_{VUV}}\right)\langle X\ \Sigma_g^+|p_z|C\ \Pi_u\rangle(R_{eq}) \times \sum_v |\langle v_C|0_X\rangle|^2 e^{-i\omega_{v_C\ g}t}F\left(\omega_{v_C,g}\right) + \text{c.c.}, \quad (8)$$

and the evaluation of its FT is straightforward.

The ATAS spectrum computed from this simple analytical treatment is shown in Fig. 4 for cases of a single $v = 0$ vibrational level, the two vibrational levels $v = 0$ and $v = 1$, and all vibrational levels in the $C\ ^1\Pi_u$ electronic state. The corresponding results obtained from a reduced TDSE calculation in which only the first Σ_g, Π_u, and Δ_g electronic states were included are shown on the right panels in Fig. 4. As can be seen, except in the region of time delays where the VUV and NIR pulses overlap, the agreement between the two sets of calculations is very good. For the most part, therefore, the complexity of the ATAS spectrum for time delays larger than approximately 20 fs is explained in terms of the interrupted beating between the ground state and selected excited states with Π_u (or Σ_u) symmetry, whereas the nature and the magnitude of such perturbation play a secondary role.

The apparent recurrences that are observed as a function of the time delay therefore have a geometrical origin. The sharp change in the coefficient $c_v(t)$ around $t = \tau$, induced by the NIR pulse, is reflected in the spectrum as the Fourier transform of a function with characteristic duration τ. This Fourier transform exhibits a central peak at $E_v - E_g$ and satellite peaks, symmetric with respect to the former peak and separated from it by $2n\pi/\tau$, whose intensity rapidly decrease as one moves away from the central peak. This means that the ATAS spectrum exhibits absorption maxima on the hyperbolas $E_{v,\ n}(\tau) = E_v + 2n\pi/\tau$. When the hyperbolas

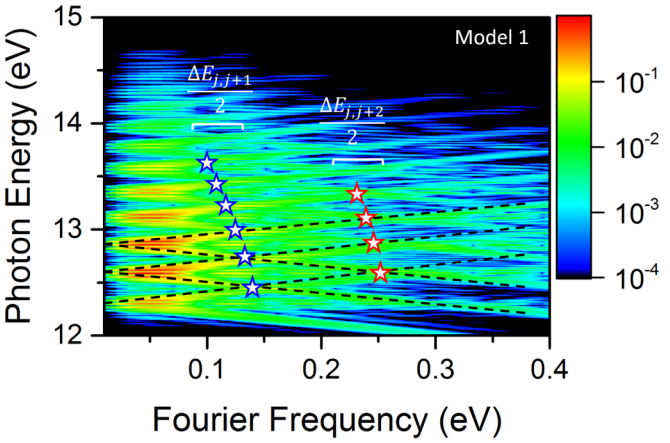

FIG. 5. Fourier transform analysis of the simulated delay-dependent absorption spectrum from Fig. 3(d). Quantum beats in the delay-dependent absorption spectrum can be observed as crossings of Fourier lines associated with different laser-perturbed vibrational states. Consecutive vibrational levels cross when the Fourier frequency is equal to half of their energy differences (blue stars), while intersections at larger Fourier frequencies indicate higher-order crossings (red stars).

from two different states intersect, e.g., in the case of two consecutive states v and $v+1$, when $E_v + 2n\pi/\tau = E_{v+1} + 2m\pi/\tau$, the maximum is amplified (middle panels in Fig. 4). From this last formula, it is immediately apparent that such amplification takes place periodically for $\tau = T_v(n-m)$, where $T_v = 2\pi/(E_{v+1} - E_v)$ is the local vibrational period (bottom panels in Fig. 4). This interpretation is confirmed by the values of the periods T_v indicated in the bottom-right panel of Fig. 4, which arise at time delays such that $n - m = 1$.

This interpretation is also confirmed by a two-dimensional (2D) spectral analysis of the ATAS spectrum resulting from our model calculations in the vicinity of the $C \leftarrow X$ transition, shown in Fig. 5. The signature of this perturbed free induction decay can be observed in the 2D spectra as lines with unity slope, intercepting the spectral axis at the energies of the unperturbed bound states (dashed lines in Fig. 5). The quantum beats observed in the delay-dependent spectrum appear at the intersection of Fourier lines associated with neighboring vibrational states. Following the model, these intersections approximately map the periods of the vibrational states in the Π_u electronic state. Consecutive vibrational levels ($\Delta v = \pm 1$) cross when the Fourier frequency is equal to half of their energy differences (blue stars in Fig. 5), resulting in the prominent beats observed in the experiments, and higher-order beats can be observed at larger Fourier frequencies where laser-perturbed vibrational levels differing by $\Delta v = \pm 2$ intersect (red stars in Fig. 5).

The $\sim$1 fs beating in the ATAS can also be understood in terms of the limited set of electronic and vibrational states presented in Sec. II. The beatings of the $B\,^1\Sigma_u^+$ absorption

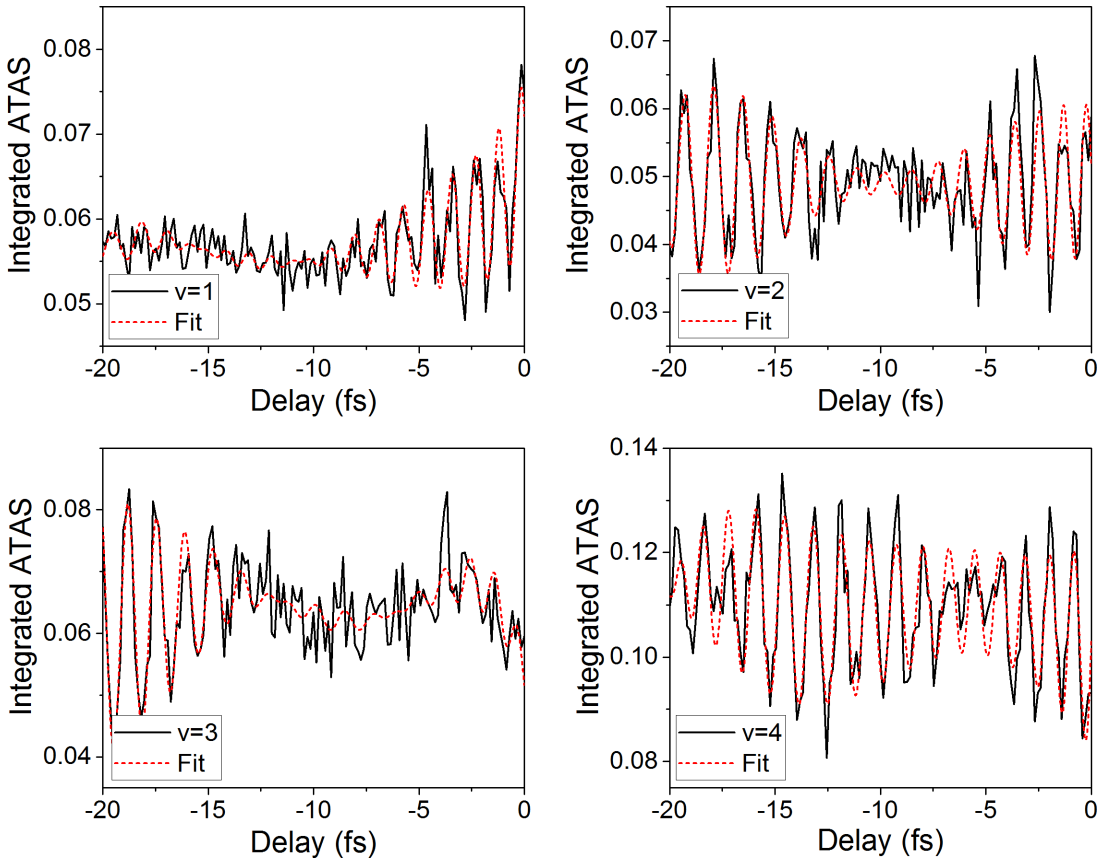

FIG. 6. Integral transient absorption cross sections of the first four vibrational peaks in the $B\,^1\Sigma_u^+$ band observed in the experimentally measured spectrum (black curves). The red dashed curves show the fits to the experimental data, allowing extraction of the local amplitudes and phases.

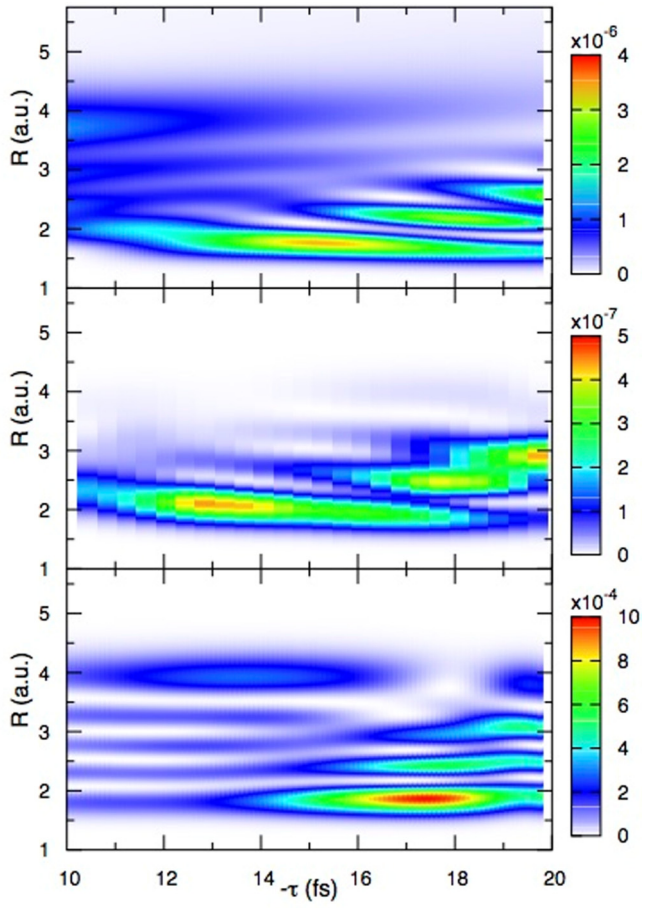

FIG. 7. Reconstruction of the nuclear wave packet in an excited electronic state. Top: Nuclear wave packet in the B' state generated by the VUV pulse. Middle: Reconstruction of this nuclear wave packet from the *ab initio* ATAS using the model described in the text. Bottom: Reconstruction of the same nuclear wave packet from the measured ATAS.

lines, observed in the spectrum between 11 and 12 eV, result from the interference between two different paths: (i) direct excitation from the ground state and (ii) stimulated emission of two NIR photons from all the $B'\,{}^1\Sigma_u{}^+$ states populated by the VUV, whose contributions add up coherently (see Fig. 1). Thus, as discussed in Sec. II, in the hypothesis that the probability amplitude for the latter two-photon transition does not depend on R, the instantaneous beating amplitudes $A_v(\tau)$ and phases $\varphi_v(\tau)$ of the $B\,{}^1\Sigma_u{}^+$ absorption features allow one to reconstruct the $B'\,{}^1\Sigma_u{}^+$ vibronic wave packet $|\nu_{B'}\rangle$ generated by the VUV pulse in terms of the stationary vibrational states $|\nu_B\rangle$ of the $B\,{}^1\Sigma_u{}^+$ potential. To illustrate this point, we fit each absorption line v associated with the B states to the simple formula $f_v(\tau) = B_v(\tau) + A_v(\tau)\cos[\omega\tau + \varphi_v(\tau)]$, where $B_v(\tau)$ is a smooth background, while $A_v(\tau)$ and $\varphi_v(\tau)$ are independent fitting parameters that depend on the time delay τ. The fits to the experimental data for several vibrational levels are shown in Fig. 6.

From this fit, we have reconstructed the nuclear wave packet in the $B'\,{}^1\Sigma_u{}^+$ electronic state as $|\nu_{B'}\rangle = \sum_v |\nu_B\rangle A_v(t)e^{i\varphi_v(t)}$. Figure 7 shows a comparison between the actual nuclear wave packet resulting from fully *ab initio* TDSE calculations performed in the absence of the NIR pulse and the nuclear wave packet reconstructed from both the *ab initio* and measured ATAS. With the exception of small time delays, for which the pump and probe pulses still partly overlap and thus our simplifying assumptions are not justified, for time delays between -10 and -20 fs, the reconstruction from the theoretical spectrum is very good. Indeed, despite the instrumental uncertainties, the reconstruction from the experimental spectrum reproduces all the main features of the rebounding wave packet.

VI. CONCLUSION

ATAS has proven valuable to the study of wave-packet dynamics and electron correlation in excited states of atoms and condensed matter. Here, we demonstrate its applicability to probing and reconstructing the electronic and nuclear dynamics in hydrogen molecules, with high temporal and spectral resolution. The ATAS measurements are capable of resolving dynamics on multiple potential energy surfaces with subfemtosecond time resolution and state selectivity, and they suggest ATAS as a suitable platform for attosecond measurement in the first steps of a photochemical reaction.

ACKNOWLEDGMENTS

This material is based on work supported by the DARPA PULSE program through a grant from AMRDEC under Award No. W31P4Q1310017; the Army Research Office under Awards No. W911NF-11-1-0297, No. WN911NF-14-1-0383, and No. FA9550-16-1-0013; the Air Force Office of Scientific Research under Awards No. FA9550-15-1-0037 and No. FA9550-16-1-0149; the National Science Foundation under Award No. PHY-1506345, an Advanced Grant of the European Research Council XCHEM 290853; and European Grants MC-ITN CORINF, the European COST Action XLIC CM1204, the MINECO Project No. FIS2013-42002-R; and the ERA-Chemistry Project PIM2010EEC-00751. All calculations were performed at the CCC-UAM and Mare Nostrum computer centers.

[1] F. Krausz and M. Y. Ivanov, Attosecond physics, Rev. Mod. Phys. **81**, 163 (2009).

[2] J. Mauritsson, T. Remetter, M. Swoboda, K. Klunder, A. L'Huillier, K. J. Schafer, O. Ghafur, F. Kelkensberg, W. Siu, P. Johnsson, M. J. J. Vrakking, I. Znakovskaya, T. Uphues, S. Zherebtsov, M. F. Kling, F. Lepine, E. Benedetti, F. Ferrari, G. Sansone, and M. Nisoli, Attosecond Electron Spectroscopy Using a Novel Interferometric Pump-Probe Technique, Phys. Rev. Lett. **105**, 053001 (2010).

[3] S. Chen, M. J. Bell, A. R. Beck, H. Mashiko, M. Wu, A. N. Pfeiffer, M. B. Gaarde, D. M. Neumark, S. R. Leone, and K. J. Schafer, Light-induced states in attosecond transient absorption spectra of laser-dressed helium, Phys. Rev. A **86**, 063408 (2012).

[4] M. Chini, X. Wang, Y. Cheng, Y. Wu, D. Zhao, D. A. Telnov, S.-I. Chu, and Z. Chang, Sub-cycle oscillations in virtual states brought to light, Sci. Rep. **3**, 1105 (2013).

[5] Z. H. Loh, M. Khalil, R. E. Correa, R. Santra, C. Buth, and S. R. Leone, Quantum State-Resolved Probing of Strong-Field-Ionized Xenon Atoms Using Femtosecond High-Order Harmonic Transient Absorption Spectroscopy, Phys. Rev. Lett. **98**, 143601 (2007).

[6] E. Goulielmakis, Z. H. Loh, A. Wirth, R. Santra, N. Rohringer, V. S. Yakovlev, S. Zherebtsov, T. Pfeifer, A. M. Azzeer, M. F. Kling, S. R. Leone, and F. Krausz, Real-time observation of valence electron motion, Nature (London) **466**, 739 (2010).

[7] R. Santra, V. S. Yakovlev, T. Pfeifer, and Z. H. Loh, Theory of attosecond transient absorption spectroscopy of strong-field-generated ions, Phys. Rev. A **83**, 033405 (2011).

[8] A. Palacios, H. Bachau, and F Martin, Excitation and ionization of molecular hydrogen by ultrashort VUV laser pulses, Phys. Rev. A **75**, 013408 (2007).

[9] G. Sansone, F. Kelkensberg, J. F. Perez-Torres, F. Morales, M. F. Kling, W. Siu, O. Ghafur, P. Johnsson, M. Swoboda, E. Benedetti, F. Ferrari, F. Lepine, J. L. Sanz-Vicario, S. Zherebtsov, I. Znakovskaya, A. L'Huillier, M. Y. Ivanov, M. Nisoli, F. Martin, and M. J. J. Vrakking, Electron localization following attosecond molecular photoionization, Nature (London) **465**, 763 (2010).

[10] P. Ranitovic, C. W. Hogle, P. Riviere, A. Palacios, X. M. Tong, N. Toshima, A. Gonzalez-Castrillo, L. Martin, F. Martin, M. M. Murnane, and H. Kapteyn, Attosecond vacuum UV coherent control of molecular dynamics, Proc. Natl. Acad. Sci. USA **111**, 912 (2014).

[11] M. Chini, K. Zhao, and Z. Chang, The generation, characterization and applications of broadband isolated attosecond pulses, Nat. Photon. **8**, 178 (2014).

[12] L. Gallmann, C. Cirelli, and U. Keller, Attosecond science: recent highlights and future trends, Annu. Rev. Phys. Chem. **63**, 447 (2012).

[13] F. Lepine, M. Y. Ivanov, and M. J. J. Vrakking, Attosecond molecular dynamics: Fact or fiction? Nat. Photon. **8**, 195 (2014).

[14] F. Lepine, G. Sansone, and M. J. J. Vrakking, Molecular applications of attosecond laser pulses, Chem. Phys. Lett. **578**, 1 (2013).

[15] N. de Oliveira, M. Roudjane, D. Joyeux, D. Phalippou, J.-C. Rodier, and L. Nahon, High-resolution broad-bandwidth Fourier-transform absorption spectroscopy in the VUV range down to 40 nm, Nat. Photon. **5**, 149 (2011).

[16] Z. H. Loh and S. R. Leone, Ultrafast strong-field dissociative ionization dynamics of CH_2Br_2 probed by femtosecond soft x-ray transient absorption spectroscopy, J. Chem. Phys. **128**, 204302 (2008).

[17] A. R. Beck, B. Bernhardt, E. R. Warrick, M. X. Wu, S. Chen, M. B. Gaarde, K. J. Schafer, D. M. Neumark, and S. R. Leone, Attosecond transient absorption probing of electronic superpositions of bound states in neon: Detection of quantum beats, New J. Phys. **16**, 113016 (2014).

[18] E. R. Warrick, W. Cao, D. M. Neumark, and S. R. Leone, Probing the dynamics of Rydberg and valence states of molecular nitrogen with attosecond transient absorption spectroscopy, J. Phys. Chem. A **120**, 3165 (2016).

[19] B. Bernhardt, A. R. Beck, X. Li, E. R. Warrick, M. J. Bell, D. J. Haxton, C. W. McCurdy, D. M. Neumark, and S. R. Leone, High-spectral-resolution attosecond absorption spectroscopy of autoionization in xenon, Phys. Rev. A **89**, 023408 (2014).

[20] Z. H. Loh, C. H. Greene, and S. R. Leone, Femtosecond induced transparency and absorption in the extreme ultraviolet by coherent coupling of the He 2s2p ($^1P^o$) and $2p^2$ ($^1S^e$) double excitation states with 800 nm light, Chem. Phys. **350**, 7 (2008).

[21] H. Wang, M. Chini, S. Chen, C.-H. Zhang, F. He, Y. Cheng, Y. Wu, U. Thumm, and Z. Chang, Attosecond Time-Resolved Autoionization of Argon, Phys. Rev. Lett. **105**, 143002 (2010).

[22] C. Ott, A. Kaldun, L. Argenti, P. Raith, K. Meyer, M. Laux, Y. Z. Zhang, A. Blattermann, S. Hagstotz, T. Ding, R. Heck, J. Madronero, F. Martin, and T Pfeifer, Reconstruction and control of a time-dependent two-electron wave packet, Nature (London) **516**, 374 (2014).

[23] M. Schultze, E. M. Bothschafter, A. Sommer, S. Holzner, W. Schweinberger, M. Fiess, M. Hofstetter, R. Kienberger, V. Apalkov, V. S. Yakovlev, M. I. Stockman, and F Krausz, Controlling dielectrics with the electric field of light, Nature (London) **493**, 75 (2013).

[24] M. Schultze, K. Ramasesha, C. D. Pemmaraju, S. A. Sato, D. Whitmore, A. Gandman, J. S. Prell, L. J. Borja, D. Prendergast, K. Yabana *et al.*, Attosecond band-gap dynamics in silicon, Science **346**, 1348 (2014).

[25] B. J. Sussman, D. Townsend, M. Y. Ivanov, and A. Stolow, Dynamic Stark control of photochemical processes, Science **314**, 278 (2006).

[26] F. Calegari, D. Ayuso, A. Trabattoni, L. Belshaw, S. De Camillis, S. Anumula, F. Frassetto, L. Poletto, A. Palacios, P. Decleva, J. B. Greenwood, F. Martín, and M Nisoli, Ultrafast electron dynamics in phenylalanine initiated by attosecond pulses, Science **346**, 336 (2014).

[27] E. Romero, R. Augulis, V. I. Novoderezhkin, M. Ferretti, J. Thieme, D. Zigmantas, and R van Grondelle, Quantum coherence in photosynthesis for efficient solar-energy conversion, Nat. Phys. **10**, 676 (2014).

[28] X. Feng, S. Gilbertson, H. Mashiko, H. Wang, S. D. Khan, M. Chini, Y. Wu, K. Zhao, and Z. Chang, Generation of Isolated Attosecond Pulses with 20 to 28 Femtosecond Lasers, Phys. Rev. Lett. **103**, 183901 (2009).

[29] X. Wang, M. Chini, Y. Cheng, Y. Wu, and Z Chang, In situ calibration of an extreme ultraviolet spectrometer for attosecond transient absorption experiments, Appl. Opt. **52**, 323 (2013).

[30] L. Argenti, Á. Jiménez-Galán, C. Marante, C. Ott, T. Pfeifer, and F. Martín, Dressing effects in the attosecond transient absorption spectra of doubly excited states in helium, Phys. Rev. A **91**, 061403 (2015).

[31] J. L. Sanz-Vicario, H. Bachau, and F. Martin, Time-dependent theoretical description of molecular autoionization produced by femtosecond XUV laser pulses, Phys. Rev. A **73**, 033410 (2006).

[32] T. E. Sharp, Potential-energy curves for molecular hydrogen and its ions, At. Data Nucl. Data Tables **2**, 119 (1970).

[33] G. R. Cook and P. H. Metzger, Photoionization and absorption cross sections of H_2 and D_2 in the vacuum ultraviolet region, J. Opt. Soc. Am. **54**, 968 (1964).

[34] W. F. Chan, G. Cooper, and C. E. Brion, Absolute optical oscillator-strengths for the electronic excitation of atoms at high resolution: Experimental methods and measurements for helium, Phys. Rev. A **44**, 186 (1991).

[35] Z. P. Zhong, W. H. Zhang, K. Z. Xu, R. F. Feng, and J. M. Li, Experimental and theoretical study of photoabsorption spectra of molecular hydrogen in the energy region 11–19 eV, Phys. Rev. A **60**, 236 (1999).

[36] A. N. Pfeiffer, M. J. Bell, A. R. Beck, H. Mashiko, D. M. Neumark, and S. R. Leone, Alternating absorption features during attosecond-pulse propagation in a laser-controlled gaseous medium, Phys. Rev. A **88**, 051402 (2013).

[37] C. T. Liao, A. Sandhu, S. Camp, K. J. Schafer, and M. B. Gaarde, Beyond the Single-Atom Response in Absorption Line Shapes: Probing a Dense, Laser-Dressed Helium Gas with Attosecond Pulse Trains, Phys. Rev. Lett. **114**, 143002 (2015).

[38] C. T. Liao, A. Sandhu, S. Camp, K. J. Schafer, and M. B. Gaarde, Attosecond transient absorption in dense gases: Exploring the interplay between resonant pulse propagation and laser-induced line-shape control, Phys. Rev. A **93**, 033405 (2016).

[39] S. H. Autler and C. H. Townes, Stark effect in rapidly varying fields, Phys. Rev. **100**, 703 (1955).

[40] C. H. Brito-Cruz, J. P. Gordon, P. C. Becker, R. L. Fork, and C. V. Shank, Dynamics of spectral hole burning, IEEE J. Quant. Electron. **24**, 261 (1988).

[41] M. Chini, X. W. Wang, Y. Cheng, and Z. H. Chang, Resonance effects and quantum beats in attosecond transient absorption of helium, J. Phys. B: At. Mol. Opt. Phys. **47**, 124009 (2014).

[42] A. R. Beck, D. M. Neumark, and S. R. Leone, Probing ultrafast dynamics with attosecond transient absorption, Chem. Phys. Lett. **624**, 119 (2015).

[43] M. Born and R. Oppenheimer, Zur Quantentheorie der Molekeln, Ann. Phys. (Berlin) **389**, 457 (1927).

[44] J. E. Baekhoj, L. Yue, and L. B. Madsen, Nuclear-motion effects in attosecond transient-absorption spectroscopy of molecules, Phys. Rev. A **91**, 043408 (2015).